Role of meteorological variability in global tropospheric ozone during 1970–2008

Takashi Sekiya[1] and Kengo Sudo[1]

Received 4 May 2012; revised 18 July 2012; accepted 14 August 2012; published 21 September 2012.

[1] Interannual variation in global tropospheric ozone associated with meteorological variability is characterized in this study using a global chemical transport model CHASER. We focus on five meteorological variability: El Niño Southern Oscillation (ENSO), Indian Ocean Dipole (IOD), Arctic Oscillation (AO), Hadley, and monsoon circulations. Results show that the anomaly in tropospheric column ozone (TCO) is positive (1–1.5 DU) in the western Pacific including Indonesia and negative (−2.5 DU) in the eastern Pacific in October–November–December (OND) during positive phase of ENSO. The model exhibits TCO increase (0.5–1.5 DU) in the central to eastern Pacific over the subtropics. During the positive phase of IOD, the model shows TCO increase (1.5–2 DU) in the west of 90°E with a decrease (1–1.5 DU) in the east. Intensified Hadley circulation causes TCO increase (0.8 DU) in North America in DJF. Intensified monsoon circulation enhances TCO (1.2 DU) in the western Indian Ocean. During positive phase of AO, TCO is decreased (1 DU) in the high northern latitudes. The contribution of meteorological variability to total interannual variation in global and regional TCO is also quantified in this study. The results suggest that interannual variation of TCO in the tropics and high northern latitudes are generally explainable by ENSO, IOD, AO, and interannual variation in Hadley and monsoon circulations. ENSO explains 79% of the variance in the tropical eastern Pacific in OND. AO explains 72% of the variance in the high northern latitudes in DJF.

Citation: Sekiya, T., and K. Sudo (2012), Role of meteorological variability in global tropospheric ozone during 1970–2008, *J. Geophys. Res.*, *117*, D18303, doi:10.1029/2012JD018054.

1. Introduction

[2] Tropospheric ozone is an important greenhouse gas, pollutant, and source of OH radicals. Its contribution to global warming from the preindustrial era to the present is regarded as the third most important, following those of carbon dioxide (CO_2) and methane (CH_4) [*Intergovernmental Panel on Climate Change*, 2007]. Elucidation of the processes determining spatial and temporal variation in global tropospheric ozone is important for evaluation of the effect of ozone on climate change because its spatial and temporal variations are more heterogeneous than that of either CO_2 or CH_4. The increased emissions of ozone precursors are recognized as a main contributor to long-term increases in tropospheric ozone from the preindustrial era to the present. However, changes in meteorology strongly influence the interannual variation of tropospheric ozone on global and regional scale [e.g., *Hess and Mahowald*, 2009; *Kurokawa et al.*, 2009; *Pozzoli et al.*, 2011]. Additionally, long-term meteorological change caused by climate change can influence future changes in tropospheric ozone [*Sudo et al.*, 2003; *Brasseur et al.*, 2006; *Zeng et al.*, 2008].

[3] Results of earlier studies suggest that interannual ozone variation is controlled substantially by meteorological variability, such as that attributable to El Niño Southern Oscillation (ENSO) and Arctic Oscillation (AO) [e.g., *Lamarque and Hess*, 2004; *Doherty et al.*, 2006]. Interannual variation of ozone induced by ENSO has been studied using both satellite observation and global models. The earliest work studied changes in tropospheric column ozone derived from satellite observations during 1997 El Niño [*Chandra et al.*, 1998]. Several modeling studies simulated changes in tropospheric ozone in 1997 to quantify the impacts of Indonesian wildfires and meteorological changes [*Sudo and Takahashi*, 2001; *Chandra et al.*, 2002]. Recently, changes in tropospheric ozone and carbon monoxide during the 2006 El Niño and the positive phase of Indian Ocean Dipole (IOD) were examined by combining measurements and model simulations [*Chandra et al.*, 2009; *Nassar et al.*, 2009; *Zhang et al.*, 2011]. Other studies characterized the response of ozone to ENSO using long-term observations and simulations [*Ziemke and Chandra*, 1999; *Peters et al.*, 2001; *Doherty et al.*, 2006; *Koumoutsaris et al.*, 2008; *Ziemke et al.*, 2010; *Oman et al.*, 2011; *Randel and Thompson*, 2011]. Results obtained from these studies suggest that changes in tropospheric ozone associated with ENSO were caused not only by extensive forest fires

[1]Graduate School of Environmental Studies, Nagoya University, Nagoya, Japan.

Corresponding author: T. Sekiya, Graduate School of Environmental Studies, Nagoya University, Furo-cho Chikusa-ku, Nagoya 464-8601, Japan. (sekiya.takashi@a.mbox.nagoya-u.ac.jp)

0148-0227/12/2012JD018054

throughout Indonesia, but also by marked changes in meteorological conditions. *Sudo and Takahashi* [2001] reported that key meteorological factors of the ozone changes are upward–downward motion, suppressed–enhanced convection, and their associated water vapor changes. However, the respective contributions of factors are not understood quantitatively.

[4] Some studies have examined the impact of Arctic oscillation (AO) on interannual variation in ozone in the northern midlatitudes to high latitudes. *Lamarque and Hess* [2004] described that AO can explain up to 50% of the ozone variation observed by ozonesonde below 500 hPa over the North American continent in spring. *Creilson et al.* [2005] found that AO correlates with the tropospheric ozone residual derived from satellites over Europe in springtime. *Hess and Lamarque* [2007] attributed changes in ozone associated with AO to four source regions: Europe, North America, Asia, and the stratosphere. They asserted that the change in ozone from the stratosphere decreases ozone throughout the troposphere over northern Canada and the Arctic, and that the regional changes in surface ozone around Europe, United States, Siberia, and East Asia are governed by changes in the transport of ozone produced in the troposphere.

[5] Effects of interannual variation in the Hadley and monsoon circulations on tropospheric ozone have been examined only cursorily. *Liu et al.* [2011] described that the Asian ozone anomaly over the Middle East correlates with two independent summer monsoon indices, suggesting that intensified Asian summer monsoon circulation also enhances the transport of Asian ozone to the Middle East. However, the impact of Asian winter monsoons on TCO has not been investigated.

[6] As described above, researchers have examined the impact of individual meteorological variability, in particular ENSO and AO, on ozone. However, interannual variation in the global distribution of tropospheric ozone is not understood comprehensively. Furthermore, understanding the interannual variability of ozone is important for testing the change in the ozone under global warming because ENSO and AO might respectively provide previews of climate warming in the tropics and the northern mid-high latitudes [*Yamaguchi and Noda*, 2006]. In this study, we investigate interannual changes in global tropospheric ozone associated with meteorological variability, and quantify the contribution of meteorological variability to total interannual variation in global and regional tropospheric ozone.

[7] Section 2 described the model and experimental settings, observational data, and analytical methods. We investigated the impacts of ENSO, IOD, AO, interannual variation in Hadley and monsoon circulations on tropospheric column ozone (TCO), and discussed their mechanisms in section 3. Their contributions to interannual variation in regional ozone are quantified in section 4. Finally, in section 5, we summarize the results and present our conclusions.

2. Methodology

2.1. Global Chemical Transport Model

2.1.1. Model Description

[8] We employ the CHASER global chemical transport model [*Sudo et al.*, 2002], which was developed in the framework of the Center of Climate System Research (CCSR)/ National Institute of Environmental Studies (NIES)/ Frontier Research Center of Global Change (FRCGC) AGCM. This study adopts a horizontal resolution of T42 (about $2.8^\circ \times 2.8^\circ$) with 32 vertical layers from the surface to about 40 km altitude. Advective transport is calculated using a fourth-order flux-form advection scheme of the monotonic Van Leer [*Van Leer*, 1977]. Convective transport is also simulated in the framework of the cumulus convection scheme (prognostic Arakawa–Schubert scheme).

[9] CHASER calculates the gas-phase and liquid-phase chemistry and heterogeneous reactions (53 species and 154 reactions) including the O_3-HO_x-NO_x-CH_4-CO system and oxidation of non-methane hydrocarbon. Dry deposition [*Wesely*, 1989] and wet deposition (cloud-out and rain-out) processes are also included.

[10] To extract the impact of interannual variation in transport on tropospheric ozone, we also use the framework of a tagged ozone simulation [*Sudo and Akimoto*, 2007]. The tagged ozone simulation calculates the temporal evolution of a hypothetical ozone tracer using the archived three-hourly production rate and loss frequency of the odd oxygen family (O_x = O_3 + O + O (^{1}D) + NO_2 + $2NO_3$ + $3N_2O_5$ + PANs + HNO_3 + other nitrates). Ozone accounts for more than 95% of O_x family in remote regions, although it accounts for 70–90% in the polluted regions. The difference between ozone and O_x induces error, because dry and wet depositions of tagged tracer are calculated as ozone. For example, HNO_3 which is counted as O_x induces error through wet deposition process. Therefore, the production rate in the boundary layers is scaled according to ratio of ozone to O_x for reducing the difference. By contrast loss rate in the boundary layer is not scaled, because most of O_x chemical loss are occupied by three reactions; $O^1D + H_2O$, $O_3 + HO_2$, and O_3 + OH.

2.1.2. Past Simulation

[11] We performed simulations for the 39 years of 1970–2008 (hereinafter S1). Meteorological fields (horizontal wind and temperature) in CHASER are relaxed to 12 hourly National Center of Environmental Prediction/National Center of Atmospheric Research (NCEP/NCAR) reanalysis data [*Kalnay et al.*, 1996]. The simulation uses the Hadley Centre's Sea Ice and Sea Surface Temperature data set (HadISST) [*Rayner et al.*, 2003].

[12] In the simulation, emissions of ozone precursors do not vary year to year (except lightning NO_x), which facilitates evaluation of the impact of year-to-year variation in meteorology on tropospheric ozone apart from that of year-to-year variation in emissions. However, anthropogenic and biomass burning emissions include only decadal changes. Anthropogenic emissions are based on EDGAR HYDE [*van Aardenne et al.*, 2001] and 3.2 FT2000 [*Olivier et al.*, 2005]. Biomass burning emissions are from GFED ver. 2 [*van der Werf et al.*, 2006]. We constructed biomass burning emission assuming that (1) its annual amount has decadal variation in proportion to the population in the corresponding region, (2) its burned location and timing are maintained at 2001 levels. Our constructed CO emission shows positive trend slightly larger than RETRO emission in the tropics where biomass burning occupy a half of total emission. We chose 2001 as the base year of timing and location, because biomass burning in Indonesia was not influenced by ENSO. However, global total emission from biomass burning in 2001 was larger than average during 1997–2004

[*van der Werf et al.*, 2006]. The larger emission was mainly responsible for emissions in Africa and Australia. Therefore, we need to interpret our model result with caution. The simulation includes natural sources of NO_x from soil (5 TgN/yr) and lightning (about 5 TgN/yr). The amount derived from lightning varies from year to year because it is parameterized in the framework of cumulus convection scheme according to *Price and Rind* [1992]. Biogenic emissions of isoprene (400 TgC/yr) and terpenes (100 TgC/yr) are calculated according to *Sudo and Akimoto* [2007]. Because we focus on direct impact of meteorological variability on transport and chemistry processes, we adopted monthly mean climatology of biogenic emission.

[13] The ozone concentration above 20 km is relaxed to the prescribed data at each grid. The data is based on monthly climatological distribution of Halogen Occultation Experiment project (HALOE) and decadal change estimated from equivalent effective stratospheric chlorine (EESC). Therefore, the ozone above 20 km does not include interannual variation due to meteorological variability. Additionally, zonal mean ozone between tropopause and 20 km is relaxed to that of the data. The prescribed NO_y data are output from a three-dimensional stratospheric chemistry model [*Takigawa et al.*, 1999].

2.1.3. Simulation Fixed to Chemical Field in 1990

[14] Interannual variation in meteorology influences the tropospheric ozone distribution through both transport (advection, convection, and diffusion) and chemical (production and loss) processes. To isolate the impact of interannual variation in transport on ozone, we performed a simulation fixed to the 1990 chemical field (chemical production and loss rate of O_x) for 39 years (hereinafter S2). The chemical field in 1990 is not largely influenced by meteorological variability, because all indices for 1990 do not exceed to one standard deviation (Figure 1). The ozone tendency at each grid is written as

$$\frac{dC}{dt} = \left(\frac{dC}{dt}\right)_{transport} + \left(\frac{dC}{dt}\right)_{drydeposition} + P - \beta C, \qquad (1)$$

where C stands for the ozone concentration, P denotes the ozone production rate, β signifies the ozone loss rate, and subscripts denote processes. In this simulation, we maintained the chemical production rate (P) and loss rate (β), and allowed the other tendencies (first and second term) to vary among years. A similar approach was used by *Liu et al.* [2011].

[15] We simultaneously calculated separate ozone tracers from 23 regions using the 1990 chemical field. Although chemical loss of each tracer is calculated using archived loss rate everywhere in the model domain, chemical production of each tracer is calculated only inside its corresponding region. The regions were defined following as *Sudo and Akimoto* [2007]; 14 planetary boundary regions (defined as lowermost 7 model layers), 9 free troposphere regions. Additionally, ozone tracer of stratospheric origin was calculated by setting it equal to ozone (ozone from all regions) in stratosphere at each time step.

2.2. Observational Data

[16] We evaluate the performance of CHASER with satellite and ozonesonde observations. Interannual variation in global tropospheric column ozone distribution is evaluated using satellite observations from the Tropospheric Emission Spectrometer (TES). TES is a Fourier transform IR emission spectrometer [*Beer et al.*, 2001] on Aura. TES retrieval is based on the optimal estimation approach [*Rodgers*, 2000]. Details are described by *Bowman et al.* [2006] and *Kulawik et al.* [2006]. The prior profile is taken from monthly mean ozone in blocks of $10^\circ \times 60^\circ$ simulated by MOZART model. We use the TES ver. 3 nadir-viewing measurement of ozone. We map TES swath data, which have a 5×8 km^2 footprint, to the T42 grid. TES vertical sensitivity depends on altitude. Therefore, the model results were adjusted for the sensitivity by application of the averaging kernel and constraint vector (a priori profile). The modeled ozone profile was sampled at the closest grid box and time to the measurement. Data screening criteria are given following *Zhang et al.* [2010].

[17] We also used tropospheric column ozone (TCO) data derived from the Total Ozone Mapping Spectrometer (TOMS) to evaluate the interannual variation of TCO in the tropics. The TCO is calculated using the convective cloud differential (CCD) method [*Ziemke et al.*, 1998]. In the CCD method, TCO is computed by subtracting stratospheric column ozone (SCO) from total column ozone. SCO and total column ozone were derived, respectively, from high and low reflectivity measurements. We used data for the 25 years of 1979–2005 derived from TOMS on Nimbus7 and Earth Probe.

[18] We evaluate interannual variation of TCO in North America and the northern high latitude with ozonesonde observation data. The data are from the World Ozone and Ultraviolet Data Center (WOUDC). We use data obtained from eight sites: Boulder, Huntsville, and Wallops for North America, and Resolute, Thule, Ny-Alesund, Eureka, and Alert for the high northern latitudes. In the two regions, interannual variation in ozone is largely influenced by ENSO, AO, and Hadley circulation (see section 4.2).

2.3. Analytical Methods

[19] This study investigates the impacts of meteorological variability on the interannual variation in global TCO. To quantify the impact, we calculated the linear regression and correlation coefficient of TCO with respect to index of climate variability. The regression and correlation coefficients are calculated against each index separately, because Niño3.4 index correlates with DMI significantly ($r = 0.7$). We multiplied the regression coefficient by the standard deviation of each index to express physical magnitude of change for a "typical" event. We used the Niño3.4 index and dipole mode index (DMI) [*Saji et al.*, 1999], respectively, as the ENSO and IOD index. The AO index is defined as the empirical orthogonal function (EOF) first mode of sea level pressure field in the model. The indices of Hadley and monsoon circulations were constructed following *Tanaka et al.* [2004]. The indices are calculated from the velocity potential at 200 hPa. The velocity potential is defined as

$$\nabla \cdot V_H = -\nabla \chi, \qquad (2)$$

where $\boldsymbol{V_H}$ is the horizontal wind vector, and χ denotes the

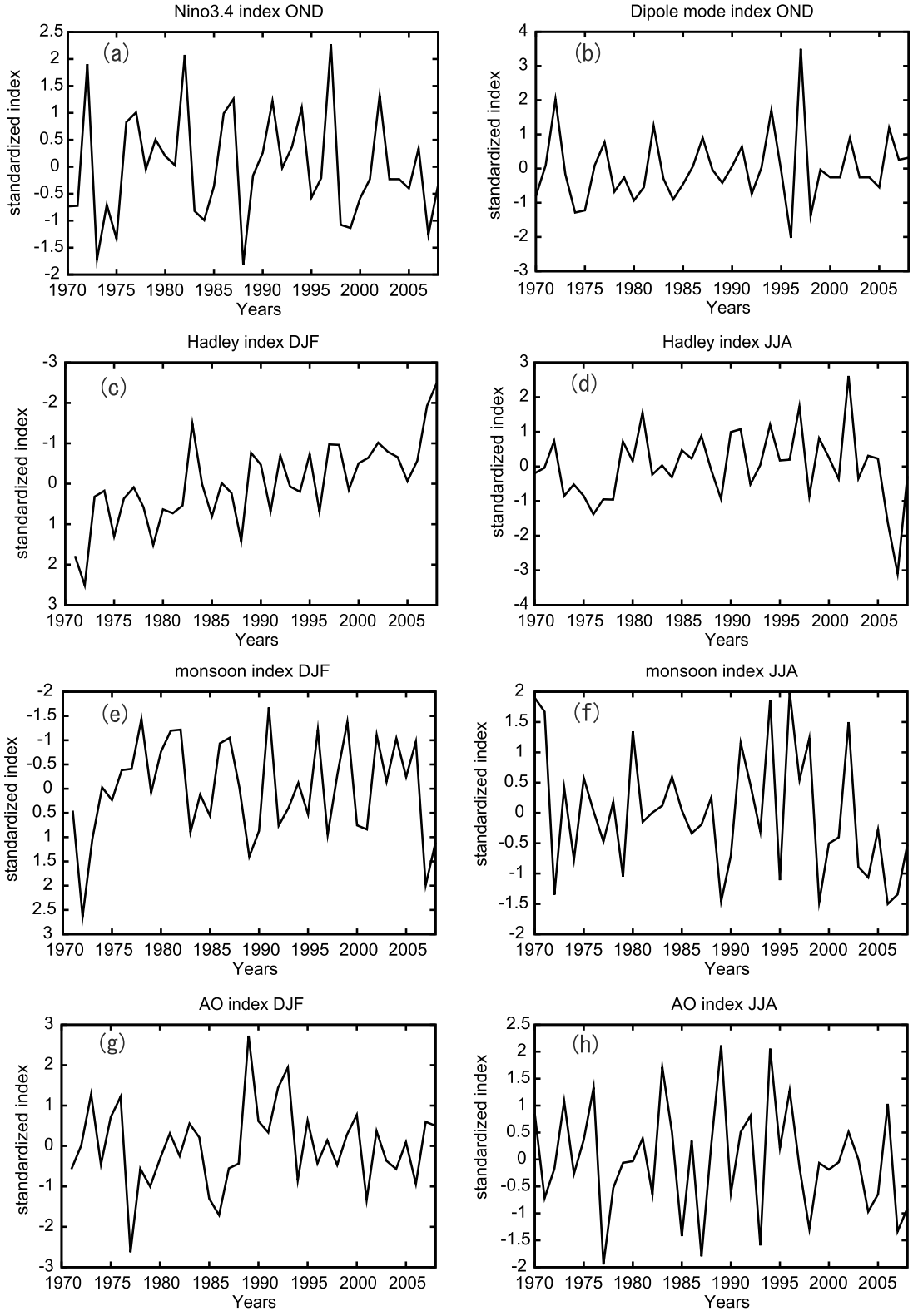

Figure 1. Indices of (a) Niño3.4, (b) Indian Ocean Dipole, (c, d) Hadley and (e, f) monsoon circulations, and (g, h) Arctic Oscillation. The indices are standardized with their +1 standard deviation. Niño3.4 and the dipole mode index are seasonal means for October–November–December (OND). Figures 1c, 1e, and 1g and Figures 1d, 1f, and 1h respectively show seasonal means for December–January–February (DJF) and for June–July–August (JJA). The y axis of Hadley and monsoon circulation indices for DJF is reversed. The details of Hadley and monsoon indices are described in *Tanaka et al.* [2004].

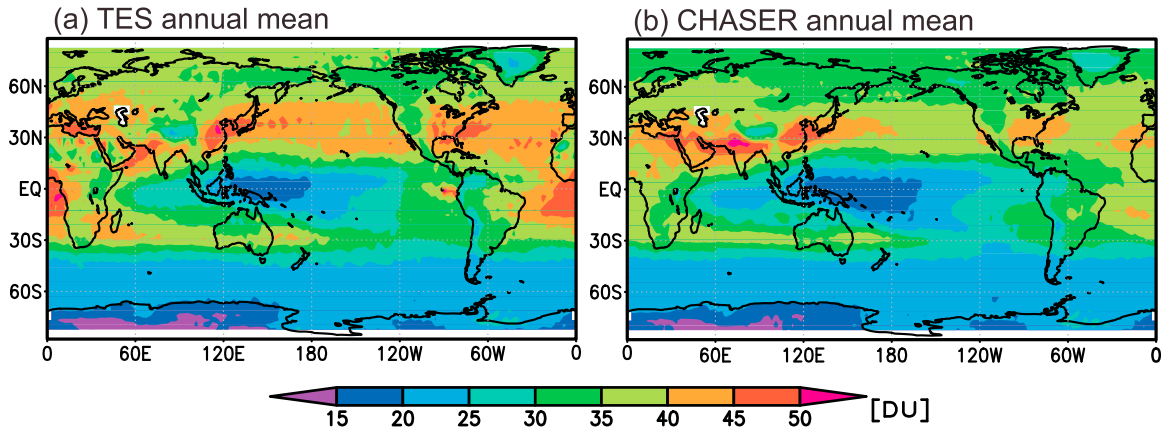

Figure 2. Annual mean distributions of tropospheric column ozone (TCO) (a) derived from TES instrument and (b) simulated by CHASER. TCO is averaged for 2005–2007. The modeled TCO was sampled at the closest grid box and time to the observation. The TES averaging kernel was applied to the modeled TCO. The unit is the Dobson Unit (DU).

velocity potential. At each grid we decompose the velocity potential into three components as,

$$\chi = [\chi] + \overline{\langle\chi\rangle} + \langle\chi\rangle', \tag{3}$$

where brackets and angle brackets are respectively zonal mean and deviation from it, and over bar and prime respectively denote one-year running mean and deviation from it. The Hadley index is defined as the minimum (maximum) value of $[\chi]$ in boreal winter (summer). The monsoon index is defined as the maximum (minimum) value of $\langle\chi\rangle'$ in boreal summer (winter). These indices can be defined only in summer and winter. Interannual variations of the indices used for this study are shown in Figure 1. The Hadley index in boreal winter shows a marked strengthening trend, which is consistent with *Tanaka et al.* [2004]. For linear regression and correlation calculation, we removed the linear trend of index and ozone in linear regression and correlation calculation to highlight year-to-year variation rather than a long-term trend.

[20] We further adopt partial correlation technique [e.g., *Spiegel*, 1988] to distinguish the impacts of ENSO and IOD on the tropospheric ozone, because the Niño3.4 index correlates closely with DMI (r = 0.7). The partial correlation coefficient $r_{AB,C}$ between variable A and B after excluding the influence of variable C is defined as

$$r_{AB,C} = \frac{r_{AB} - r_{AC}r_{BC}}{\sqrt{1 - r_{AB}^2}\sqrt{1 - r_{BC}^2}}, \tag{4}$$

where r_{AB} is the linear correlation coefficient for A and B, and so on. We calculated the partial correlation coefficients between TCO and Niño3.4 index after excluding the influence of DMI (i.e., $r_{TCONino3.4,\ DMI}$), and between TCO and DMI after excluding the influence of Niño3.4 index (i.e., $r_{TCODMI,\ Niño3.4}$).

[21] We also characterize the interannual variation of tropospheric ozone with Empirical Orthogonal Functions (EOFs). The general application of EOF analysis to the geophysical field is described by *Wilks* [2006]. We applied EOF analysis to monthly and seasonal ozone anomalies (difference from average for 1970–2008). Each meteorological variability-related signal was explored by examining the EOF spatial patterns (EOF) and the corresponding principal component time series (PC) with its index for the first four EOF modes. We multiplied EOF spatial patterns by the standard deviation of corresponding PC time series, as for the regression coefficient.

3. Interannual Variation of the Global Tropospheric Ozone Distribution

3.1. Comparison With Satellite Observation

[22] We first compare annual mean of simulated tropospheric column ozone (TCO) with that of TCO derived from the TES instrument in Figure 2. The model captures general features of TES observation. It reproduces the zonal wave-one pattern of tropical TCO with minimum of 20 DU in the western Pacific and maximum of 40 DU in the Atlantic. TCO enhancements of 40–50 DU in eastern Asia and United States are also captured well, but the enhancement in the Pacific and the Atlantic are underestimated slightly. The simulated TCO is also low-biased (6–9 DU) in the high northern latitudes. TCO peaks of South Asia and the Middle East are overestimated in the model (3–6 DU).

[23] We then evaluate interannual variation in zonal and tropical mean TCO with TES observations. A time-versus-latitude Hovmöller diagram of zonal and monthly mean TCO is portrayed in Figure 3. The monthly TCO is deseasonalized by subtracting the average during 2005–2007 in corresponding months. The modeled anomalies generally correlate with observed anomalies (r = 0.51). The correlation coefficient is significant at 99% confidence level. In high northern latitudes, the model captures observed decrease in 2006 and increase in 2007 in boreal winter. Although the observed anomaly in November and December 2007 may be related to the positive phase of AO, the modeled anomaly is not obvious. By contrast, the model does not reproduce observed anomalies in the boreal summer. The discrepancy is probably attributable to prescribed stratospheric ozone. The model underestimates ozone decrease (increase) observed by Microwave Limb Sounder/Aura (about 80%) at 100 hPa

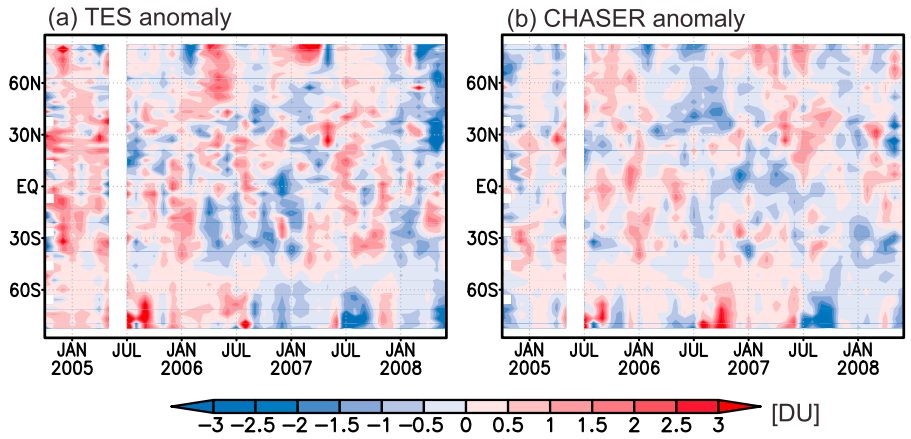

Figure 3. Time–latitude cross section of monthly and zonal mean deseasonalized TCO anomaly (DU) showing the anomaly (a) derived from TES and (b) simulated by CHASER.

during spring—early summer in 2006 (2007) in the northern mid to high latitude. The underestimation might have affected interannual variation of TCO through stratosphere to troposphere transport. TES observation also shows a negative (positive) anomaly in the tropics and positive (negative) anomalies in the subtropics in late 2006 (2007). The model reproduces these anomalies, which can be linked to ENSO and Hadley circulation.

[24] Figure 4 shows a time-versus-longitude Hovmöller diagram of monthly TCO anomaly averaged from 15°S to 15°N. The TCO is deseasonalized, as in Figure 3. The model generally captures observed anomalies (r = 0.53). The significance of correlation coefficient exceeds 99% confidence level. Both the observed and the simulated TCO changes show positive (negative) anomaly in late 2006, and negative (positive) anomalies in late 2005 and 2007 in the western Pacific and the eastern Indian Ocean (eastern Pacific). In addition, positive and negative anomalies are found, respectively, in the western Indian Ocean in late 2005 and 2006. These signals in the Pacific and the Indian Ocean can result from ENSO and IOD respectively. The simulated anomalies are smaller than the TES observations around Indonesia, primarily because of a lack of anomalous Indonesian forest fires in 2006 in the model. The model tends to capture the observed interannual variation in TCO during October–December (OND) in the tropics (r = 0.54, significant at 99% confidence level), and during December–February (DJF) in the high northern latitudes well (r = 0.53, significant at 99% confidence level). We show that ENSO, IOD, and AO can be related to interannual variation in TCO. Therefore, we investigate the impact of ENSO and IOD in OND, and ENSO and AO in DJF below. Additionally, we address interannual variation in Hadley and monsoon circulations in DJF.

3.2. Impact of El Niño–Southern Oscillation

[25] Figure 5a shows regression coefficient of TCO with respect to the Niño3.4 index in OND. A two-tail Student's t-test demonstrated that hatched regions are not significant at the 95% level. The result shows a positive anomaly of 1–1.5 DU in the tropical western Pacific including Indonesia, and a negative anomaly of 2.5 DU in the tropical eastern Pacific. The model also exhibits positive anomalies of 0.5–1.5 DU in the central to eastern Pacific over the subtropics. The correlation coefficient shows a similar pattern (not shown). Significant correlation was found in the tropical eastern Pacific (r = −0.8), Indonesia (r = 0.6) and the eastern Pacific over the subtropics (r = 0.8). These spatial patterns

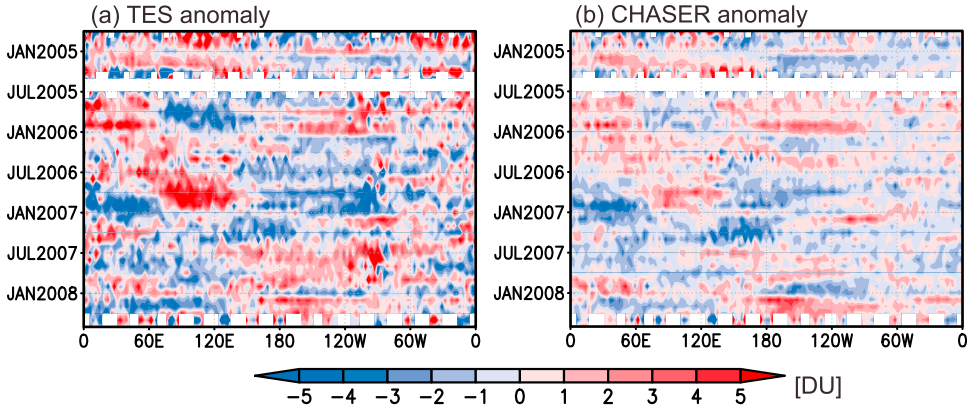

Figure 4. Longitude–time cross section of monthly deseasonalized TCO anomaly (DU) averaged between 15°S and 15°N showing the anomaly (a) derived from TES and (b) simulated by CHASER.

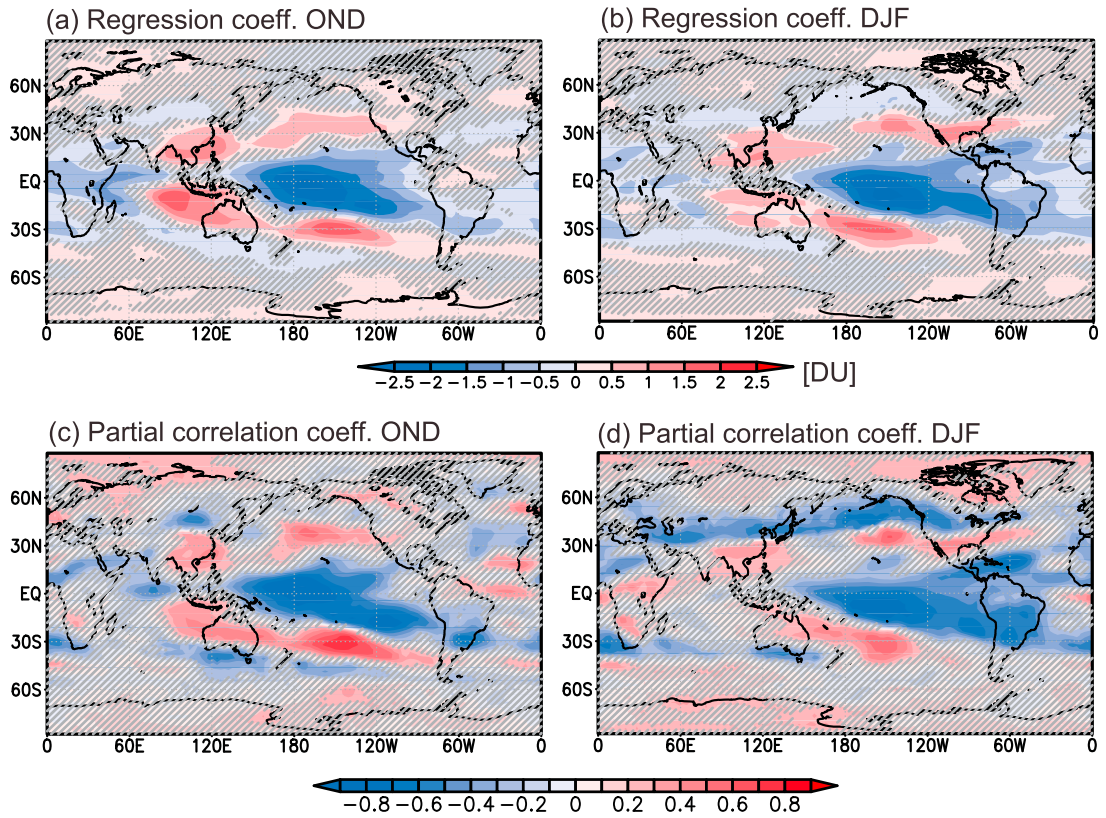

Figure 5. (a, b) Regression coefficient of TCO (DU) with respect to Niño3.4 index and (c, d) partial correlation coefficient of TCO with respect to Niño3.4 after excluding the influence of DMI. Figures 5a and 5c are calculated using TCO and the index in OND. Figures 5b and 5d are calculated using TCO in DJF and the index in OND (correspond to a 2 month lag). Hatched regions are not significant at the 95% confidence level.

are consistent with those described in earlier studies [*Doherty et al.*, 2006; *Oman et al.*, 2011].

[26] Two month-lagged regression coefficient of TCO with respect to the Niño3.4 index (i.e., regression between TCO in DJF and Niño 3.4 index in OND) is presented in Figure 5b. We picked the two month-lagged regression to compare impact of ENSO with that of Hadley circulation in southern North America in DJF. The anomalies in DJF show a similar pattern to that in OND, while positive anomaly in southern North America is elevated from 0.2 DU to 1 DU. The positive anomaly can result from the combination of an enhanced local Hadley cell and intensified subtropical jet in the eastern Pacific because of ENSO [*Shapiro et al.*, 2001; *Wang*, 2002] through changes in the horizontal and vertical transport in troposphere, and stratosphere–troposphere exchange of ozone [*Hsu et al.*, 2005].

[27] *Sudo and Takahashi* [2001] reported that large-scale atmospheric circulation, cumulus convection, and water vapor are key factors contributing to tropical TCO change during El Niño. However, the respective factors' contributions to the TCO change are not understood quantitatively. We attempt to quantify the impact of interannual variation in transport (large-scale circulation and cumulus convection) and chemistry (water vapor, etc.) associated with ENSO using the two simulations described in sections 2.1.2 and 2.1.3. S1 accommodates year-to-year variation of both meteorological (transport) and chemical fields (production and loss rate of O_x), but S2 allows only the meteorological (transport) field to vary. In this study, we define the impact of transport as regression coefficient of TCO in S2 with respect to the Niño3.4 index. We also define the impact of chemistry as regression coefficient of TCO difference between S1 and S2.

[28] Figures 6a and 6b respectively show the impacts of transport and chemistry. The impact of transport is greater than that of chemistry over most of the globe. The significant impact of chemistry is confined to the tropical central Pacific, where the impacts of transport and chemistry are comparable, although the chemistry process has less impact in Indonesia. This lesser impact is attributable to cancelling out of the positive anomaly below 5 km and negative anomaly above 5 km over Indonesia (Figures 6c and 6d). The positive anomaly (+0.2 DU) below 5 km is related to a decrease in the chemical loss of ozone with water vapor, while negative anomaly (−0.1 DU) above 5 km is related to a decrease in chemical production of ozone from lightning NO_x. However, this simulated change in lightning over Indonesia is opposite to the change derived from LIS/TRMM [*Hamid et al.*, 2001]. They showed that convective storms were concentrated on land and the coast area, and that the number of lightning flashes increased during 1997–1998 (El Niño year) compared to 1998–1999. We must improve convection and lightning NO_x schemes, for example, as did *Nassar et al.* [2009]. In addition, the impact of chemistry

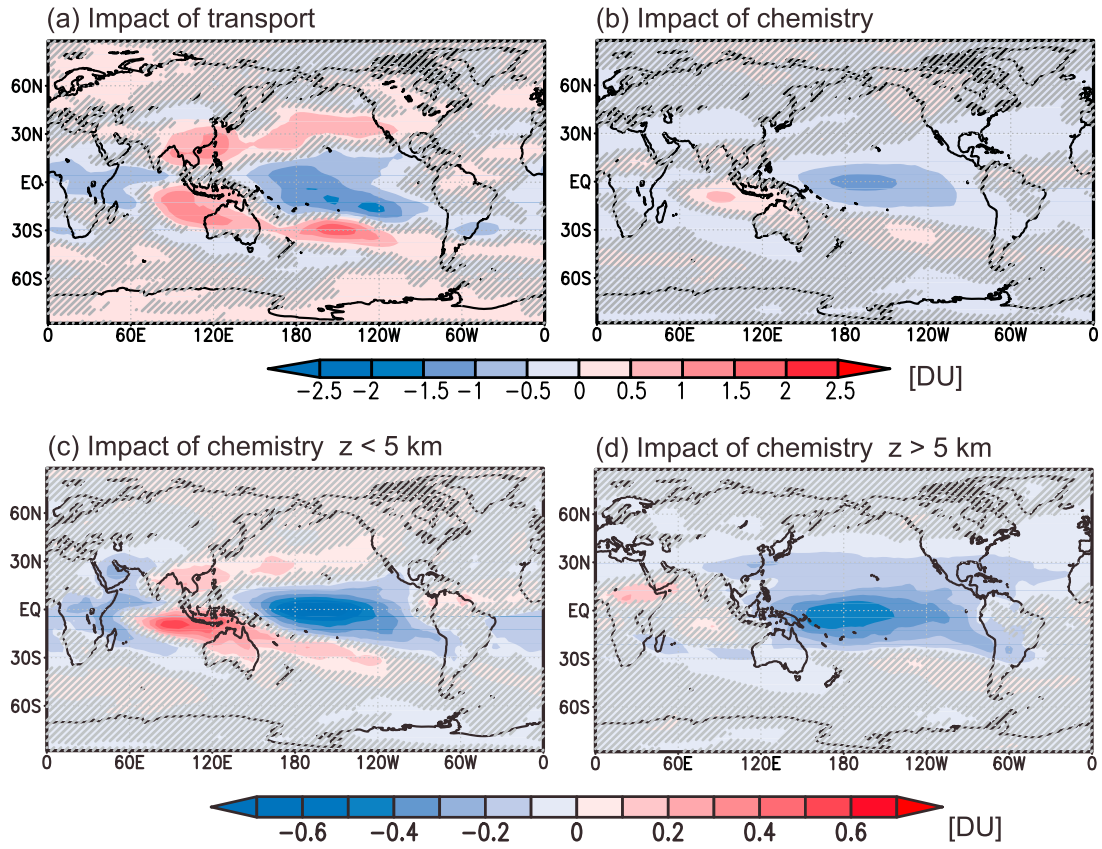

Figure 6. Impact of interannual variation in (a) transport and (b) chemistry on the regression coefficient of TCO (DU) with respect to the Niño3.4 index shown in Figure 5a, and impact of chemistry on column ozone (c) between surface and 5 km and (d) between 5 km and tropopause. The impacts are seasonal averages for OND. Hatched regions are not significant at the 95% confidence level.

may include some bias, because only one year (1990) of chemical fields is used in S2. However, as Figure 1 shows, all indices were within one standard deviation in 1990.

3.3. Impact of Indian Ocean Dipole

[29] Figure 7a presents regression coefficient with respect to DMI in OND. Positive anomaly (+1.5–2 DU) is evident in the eastern Indian Ocean and Indonesia. Negative anomaly (−1–1.5 DU) is also found in the western Indian Ocean and eastern Africa. Large-scale descent (ascent) flow, suppressed (enhanced) convection, and dryness (wetness) are found in the eastern Indian Ocean (western Indian Ocean) during the positive phase of IOD (not shown). These results suggest that the mechanism causing the changes is analogous to ENSO. We further assess the partial correlation coefficients between TCO and Niño3.4 index after removing the influence of DMI (Figure 5c) and between TCO and DMI after removing the influence of Niño3.4 index (Figure 7c), because DMI correlates significantly with the Niño3.4 index (r = 0.7). Figure 7c shows positive and negative partial correlations in the eastern and western Indian Ocean (r = 0.6 and −0.6) respectively. Although Figure 5c shows positive partial correlation between TCO and Niño3.4 in the southeastern Indian Ocean, Negative partial correlation is found along equator in the Indian Ocean. These imply that dipole structure in the Indian Ocean in Figure 7a results from IOD rather than ENSO. In the tropical eastern Pacific, negative partial correlation between TCO and DMI is weaker than that between TCO and Niño3.4 index, suggesting that the impact of ENSO is dominant.

[30] Two month-lagged regression coefficient with respect to DMI is also shown in Figure 7b as for Figure 5. Regression coefficient shows similar patterns to those with respect to Niño3.4. Figure 7d shows that two month-lagged partial correlation between TCO and DMI in the western Indian Ocean is significant (r = 0.6). However, the partial correlation between TCO and DMI in the tropical Pacific and southern North America is weaker than that between TCO and Niño3.4 index (Figures 5d and 7d).This suggests that the anomalies are due to the impact of ENSO rather than to that of IOD.

[31] We also quantify the impacts of interannual variation in transport (atmospheric circulation and convection) and chemistry (water vapor, etc.) associated with IOD on TCO as for ENSO. Figure 8 presents the impacts of transport and chemistry. The impact of transport is greater than that of chemistry as for ENSO. The significant impact of chemistry is confined to the eastern Indian Ocean. Over eastern Africa, increased ozone production from lightning NO_x and increased ozone loss with water vapor cancel each other. We need to interpret them with caution, because they may be also influenced by ENSO. Nevertheless the partial correlation in Figure 7c suggests that the anomalies are mainly caused by IOD.

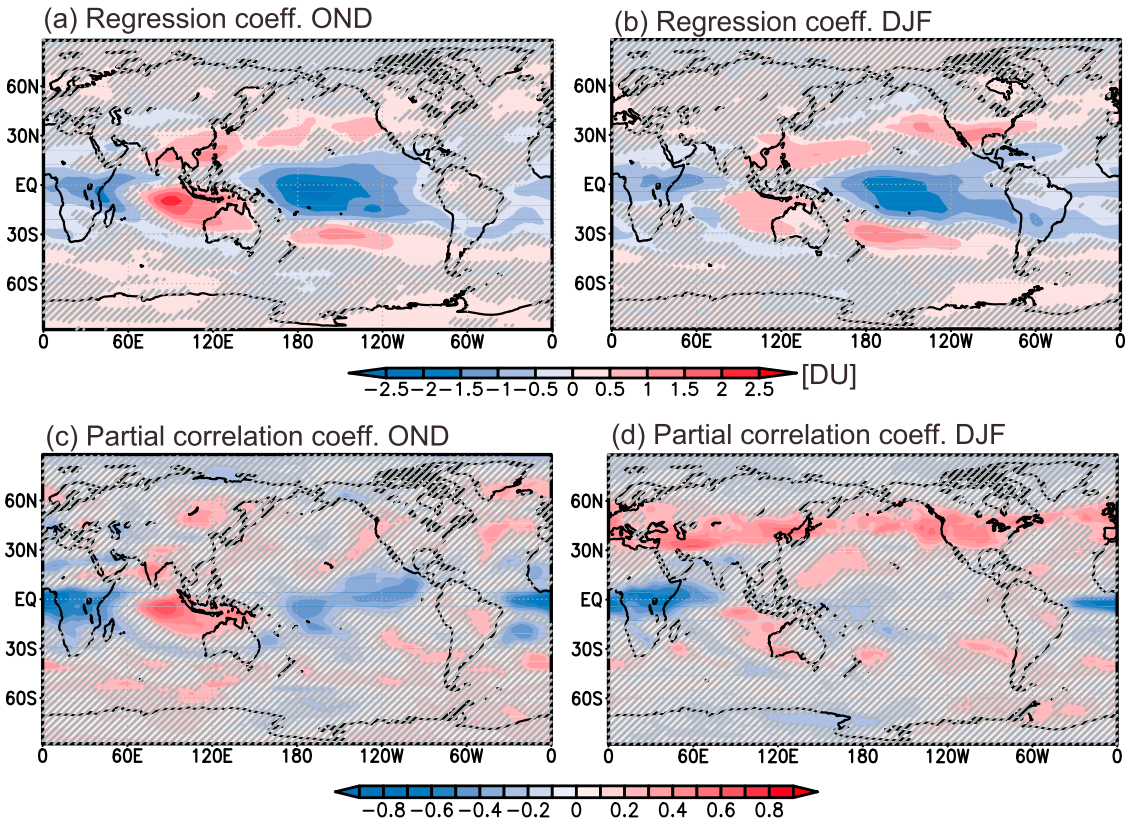

Figure 7. (a, b) Regression coefficient of TCO (DU) with respect to the dipole mode index (DMI) and (c, d) partial correlation coefficient of TCO with respect to DMI after excluding the influence of Niño3.4 index. Figures 7a and 7c are calculated using TCO and the index in OND. Figures 7b and 7d are calculated using TCO in DJF and the index in OND (corresponding to a 2 month lag). Hatched regions are not significant at the 95% confidence level.

3.4. Impact of Hadley Circulation

[32] Figure 9a presents regression coefficient of TCO with respect to the Hadley circulation index in DJF. Regression shows increases of TCO up to 0.8 DU particularly in the Himalayas, the northeast Pacific, North America, and Northern Africa. The Hadley impact is independent from ENSO because the Hadley index used for this study does not correlate with the Niño3.4 index ($r = -0.1$).

[33] We discuss the cause of change in TCO associated with Hadley circulation. Figure 9b also presents regression coefficient of TCO transported from the stratosphere. The regression coefficient shows positive anomalies (up to 0.6 DU) in the Himalayas, the northeastern Pacific, North America, and Northern Africa. The positive anomalies reach from 250 hPa to surface (Figure 9c). Additionally, Figure 9d presents climatology and regression coefficient of zonal mean vertical

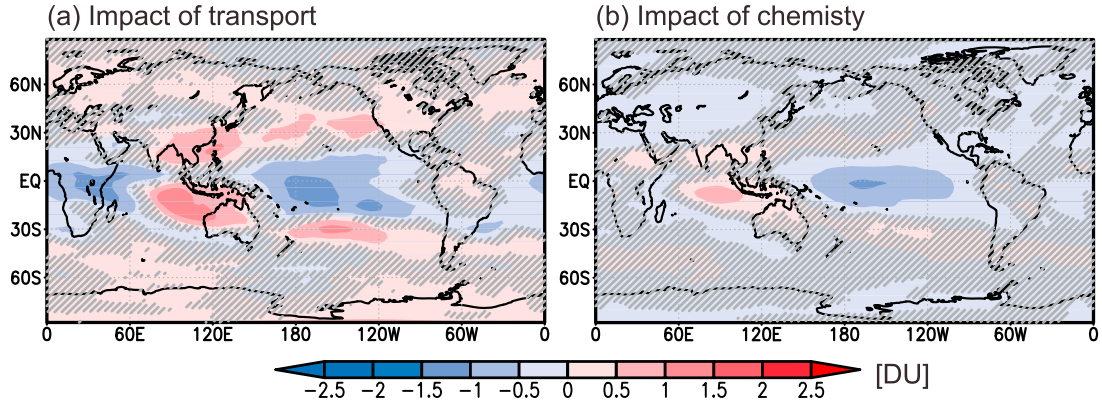

Figure 8. Impact of interannual variation in (a) transport and (b) chemistry on the regression coefficient of TCO (DU) with respect to DMI shown in Figure 7a. The impacts are seasonal averages for OND. Hatched regions are not significant at the 95% confidence level.

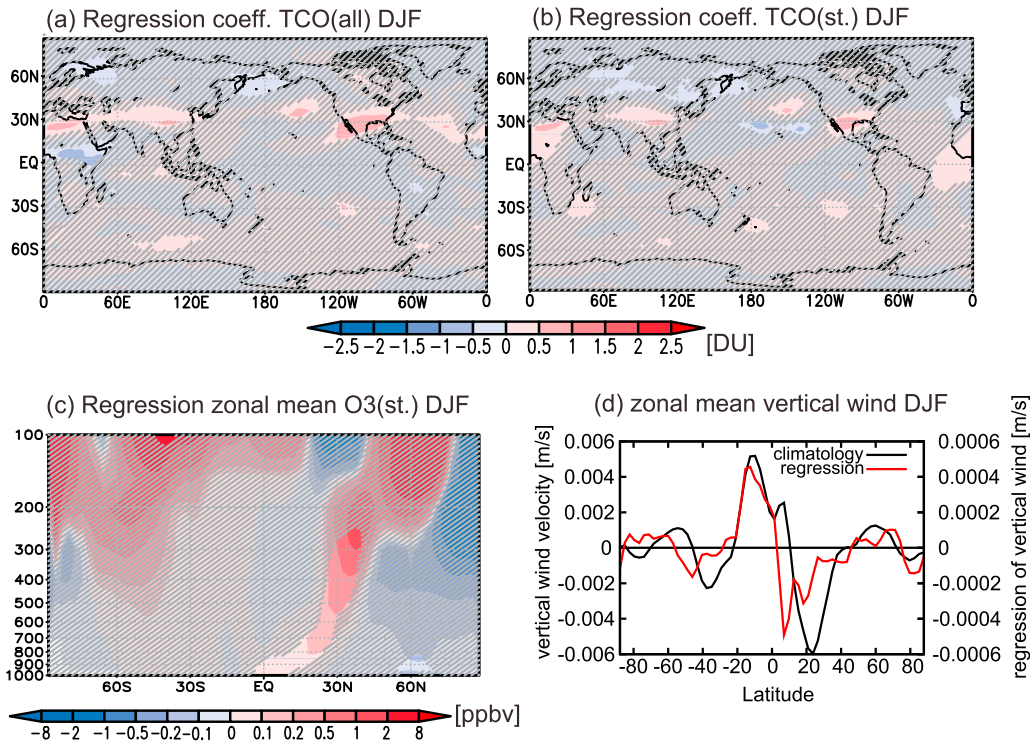

Figure 9. (a) Regression coefficient of TCO, (b) TCO transported from the stratosphere with respect to the Hadley circulation index (DU). (c) Regression of zonal mean ozone from the stratosphere with respect to Hadley circulation index (ppbv). (d) Climatology and regression coefficient of vertical wind velocity (m/s) at 300 hPa. The coefficient is calculated using TCO, ozone, or wind velocity and the index in DJF. Hatched regions are not significant at the 95% confidence level. Black and red lines respectively show climatology and regression coefficient in Figure 9d.

wind velocity at 300 hPa. The climatology and regression present increase in downward vertical wind velocity between 10°N and 40°N in upper troposphere. These results suggest that the TCO increase results from enhanced downward transport of ozone-rich air from the stratosphere and upper troposphere to the lower-middle troposphere. However, we need to investigate the reason why the anomalies are significant only in the Himalayas, the northeastern Pacific, North America, and Northern Africa.

3.5. Impact of Monsoon Circulation

[34] In this section, we particularly examine the Asian winter monsoon especially because Asian summer monsoons have a minor impact on TCO (not shown). Figures 10a and 10b present regression coefficients of TCO and horizontal wind vector at 400 hPa in DJF respectively. The regression shows positive anomaly of 1.2 DU in South Asia and the western Indian Ocean. The change in TCO results from the intensified cyclonic circulation over South

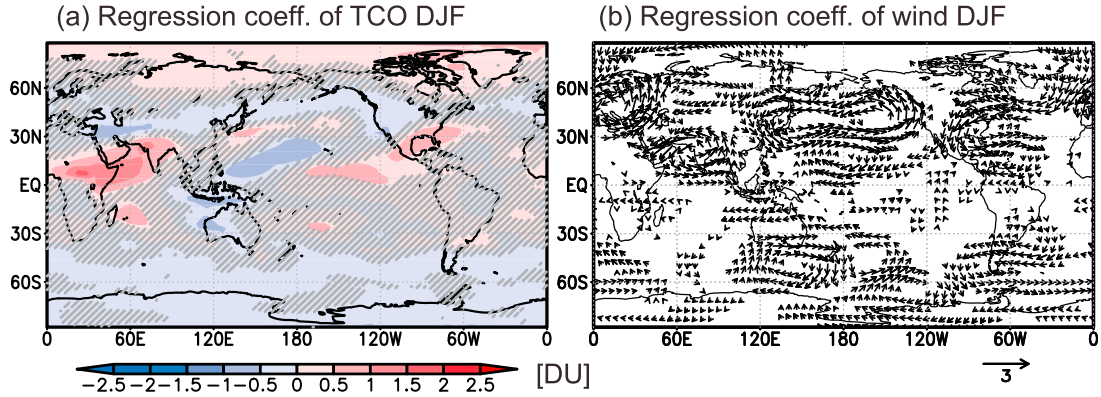

Figure 10. Regression coefficient of (a) TCO (DU) and (b) horizontal wind at 400 hPa with respect to the monsoon circulation index. The coefficient is calculated using TCO and the index in DJF. Hatched regions are not significant at the 95% confidence level. Vectors are drawn only in significant region with 95% confidence level.

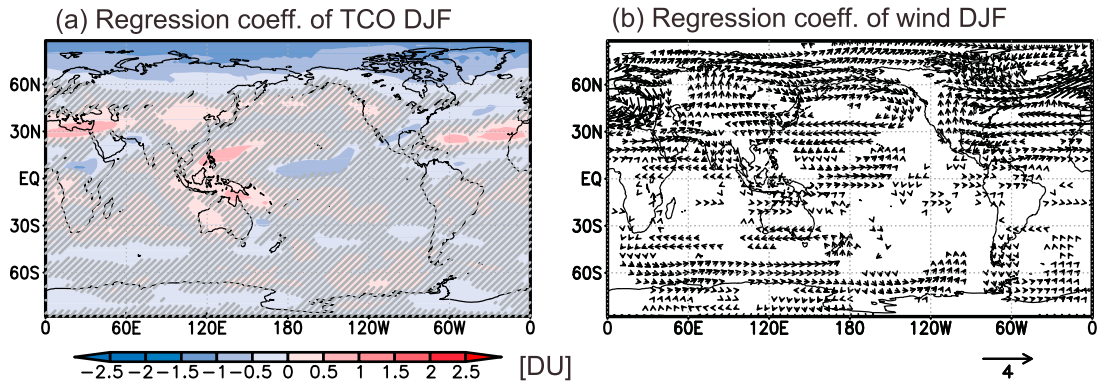

Figure 11. Regression coefficients of (a) TCO (DU) and (b) horizontal wind at 500 hPa with respect to the Arctic Oscillation index. The coefficient are calculated using TCO and the index in DJF. Hatched regions are not significant at the 95% confidence level. Vectors are drawn only in the significant region with a 95% confidence level.

Asia associated with monsoon circulation in the upper troposphere (Figure 10b). The anomalous circulation enhances transport from Africa to South Asia and the western Indian Ocean. In this study, we also calculated the tagged ozone tracers from various source regions in the simulation fixed to the 1990 chemical field. Results of the simulation suggest that ozone from North Africa (20W–52E, 0–17N) is most responsible for the TCO increase (about 40% of the increase) in the western Indian Ocean.

3.6. Impact of Arctic Oscillation

[35] Figure 11a shows regression coefficient of TCO with respect to AO index in DJF. Figure 11b shows a regression coefficient of horizontal wind at 500 hPa. Wind vectors are drawn in areas with a 95% confidence level. Figure 11a shows negative anomaly (−1 DU) in the high northern latitudes. This TCO change is qualitatively consistent with previous studies [e.g., *Hess and Lamarque*, 2007].

[36] The TCO change associated with AO is related to a change in the poleward transport from the northern midlatitude to Arctic. The poleward transport is weakened during the positive phase of AO, resulting from intensified polar vortex (Figure 11b). Our tagged ozone simulation suggests that ozone produced in the free troposphere and stratosphere is more responsible for the TCO decrease (about 95%) than that produced in the boundary layer.

4. Contribution of Meteorological Variability to Interannual Variation in Ozone

[37] In this section, we quantify the contribution of major meteorological variability to total interannual variation in global TCO (section 4.1) and regional TCO (section 4.2).

4.1. Contribution to Global Distribution

[38] We perform EOF analysis to detect the leading mode of interannual variation in global TCO and to quantify its contribution. A result of EOF analysis is shown in Figure 12. Figure 12a shows time series of EOF first mode (PC1) with the Niño3.4 index in OND. PC1 correlates with that of Niño3.4 index (r = 0.90), suggesting that the first mode represents a component related to ENSO. Spatial patterns of the first mode (EOF1) are also similar to that of the regression coefficient in Figure 5a (Figure 12b). The spatial correlation coefficient between EOF1 and the regression is 0.98. Contribution of EOF1 to total variance is 33%.

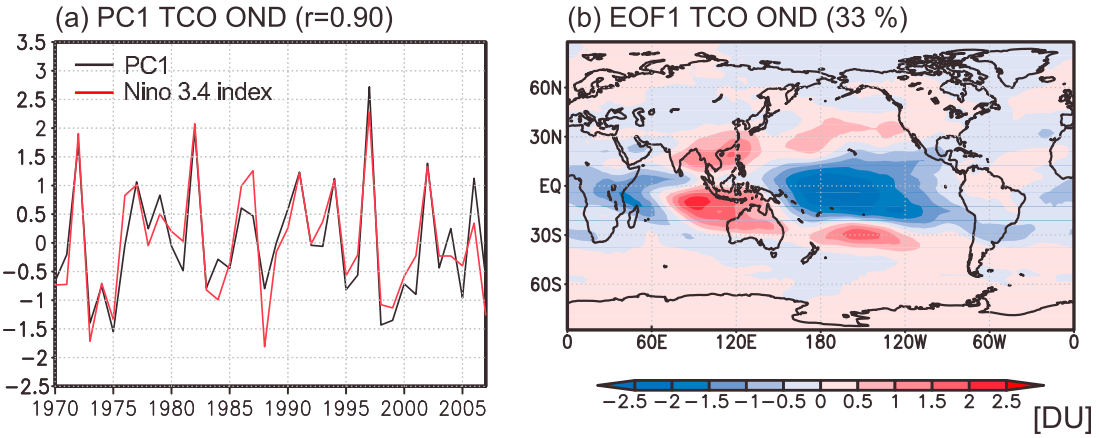

Figure 12. Time series corresponding to EOF first mode (EOF1) with Niño3.4 index. The time series are standardized with their +1 standard deviation. EOF1 eigenvector of TCO (DU) averaged for OND. The spatial pattern is scaled by +1 standard deviation of PC1. Its contribution rate is 33%.

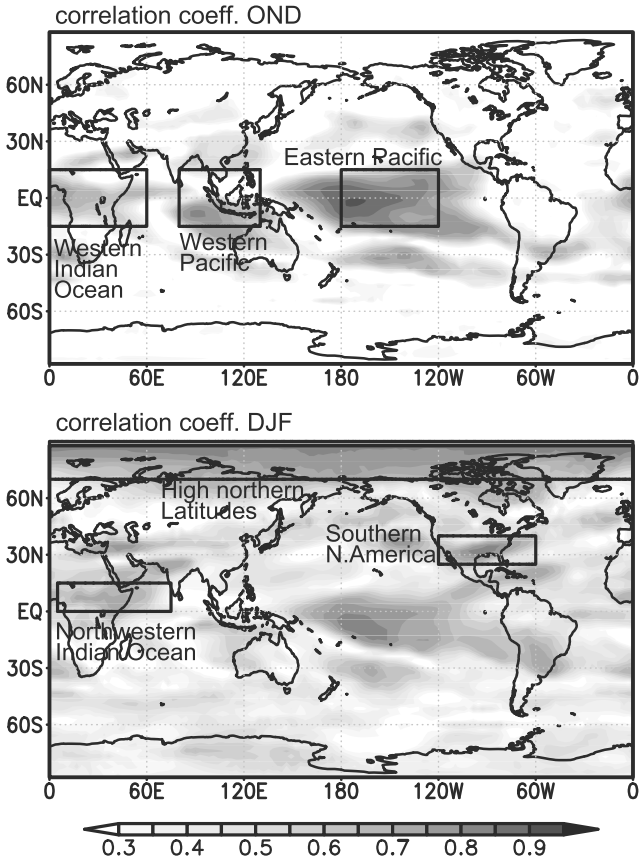

Figure 13. Correlation coefficient between the simulated TCO and total contribution of meteorological variability considered in this study, and map of regions used in Figures 14 and 15 for (top) OND and (bottom) DJF.

Hess and Mahowald [2009] also applied EOF analysis to global ozone field. Although the spatial pattern in our study is similar to that in their study, the contribution to total variance in our study is about five times larger than that in their study. This is attributable to applying EOF to TCO in OND when El Niño is mature phase. The result for DJF is also similar. These results indicate that the variation of TCO associated with ENSO is the most important in all interannual variations of global TCO distribution.

4.2. Contribution to Temporal Variation

[39] We quantify the contribution of the meteorological variability to total interannual variation of TCO in six regions. We quantify the contribution as an index of meteorological variability multiplied by the corresponding regression coefficient at each grid and year. For example, ENSO impact is given as

$$C_{ENSO}(x,y,t) = a_{ENSO}(x,y) \times I_{ENSO}(t) \quad (5)$$

where C is contribution of ENSO, a stands for regression coefficient of ENSO, I denotes Niño3.4 index, x, y, and t are longitude, latitude, and year respectively. We also constructed total contribution by adding contributions of ENSO, IOD in OND, and by adding ENSO IOD, Hadley, monsoon, and AO in DJF. Figure 13 shows correlation coefficients between the total contribution and the simulated TCO. Figure 13 (top) shows significant correlation in the eastern Pacific in the tropics, the western Pacific including Indonesia. Figure 13 (bottom) also shows the significant correlation in the southern North America and the northern high latitude as well as tropical eastern Pacific and northwestern Indian Ocean. There is, however, no significant correlation in the Atlantic, East Asia, and Europe. We focus on the six regions where the correlation coefficient is larger than 0.6 (Figure 13). The simulated TCO and the contribution of meteorological variability in the right panels of Figures 14 and 15 are detrended to emphasize year-to-year variation.

[40] Figure 14a shows the interannual variation of simulated and satellite-observed TCO in OND in the tropical eastern Pacific. The simulated variation agrees well with the observed variation, except in the late 1980s, although the model overestimates the observed long-term trend. Overestimation of the long-term trend might be attributable to increasing trend in ozone precursor emissions in the tropics after 1990 in the model. Figure 14b presents detrended TCO variation with the anomalies calculated from the Niño3.4 index (hereinafter, the ENSO component). The ENSO component, explaining 79% of the total variance (r = 0.89), is most responsible for the variation in the tropical eastern Pacific. In strong El Niño years (1982 and 1997), the ENSO component contributed more than 68% to TCO anomalies there.

[41] Figure 14c shows simulated and observed TCO anomaly in the tropical western Pacific and Indonesia. These anomalies are shown as deviations from average value during whole observation period. The average, however, does not include the value in 1997, because the simulation in this study does not include emission enhancement during the severe Indonesian fires in 1997. The model generally captures interannual variation, while the long-term trend is overestimated as in Figure 14a. Figure 14d portrays detrended TCO anomalies in addition to the anomalies calculated from the Niño3.4 index and DMI as in Figure 14b (ENSO and IOD component, respectively). In this region, both the ENSO and IOD components play important roles in the interannual variation of TCO. They contributed more than 84% of the TCO increase in 1982 and 1997. The quantities of relative importance of the ENSO and IOD components were 56% and 44%, respectively, in 1982, and were 35% and 65% in 1997. We, however, need to pay attention to possible double counting of ENSO and IOD, because of the significant correlation between Nino 3.4 index and DMI. In other El Niño years, TCO changes are not explained merely by ENSO and IOD. This results from interannual variation in ozone above 5 km, which might be related to changes occurring in the upper tropospheric circulation over Indonesia.

[42] Interannual variation of TCO in the tropical western Indian Ocean in OND is shown in Figure 14e. The satellite observation and the simulation show similar variations, especially after 1996. The simulated increasing trend is overestimated after 1990 as in the tropical Pacific. Figure 14f presents detrended anomalies that are simulated and calculated from DMI (IOD component). IOD explains 36% of TCO variation in the tropical western Indian Ocean. The variation after 1992 is particularly influenced by IOD significantly.

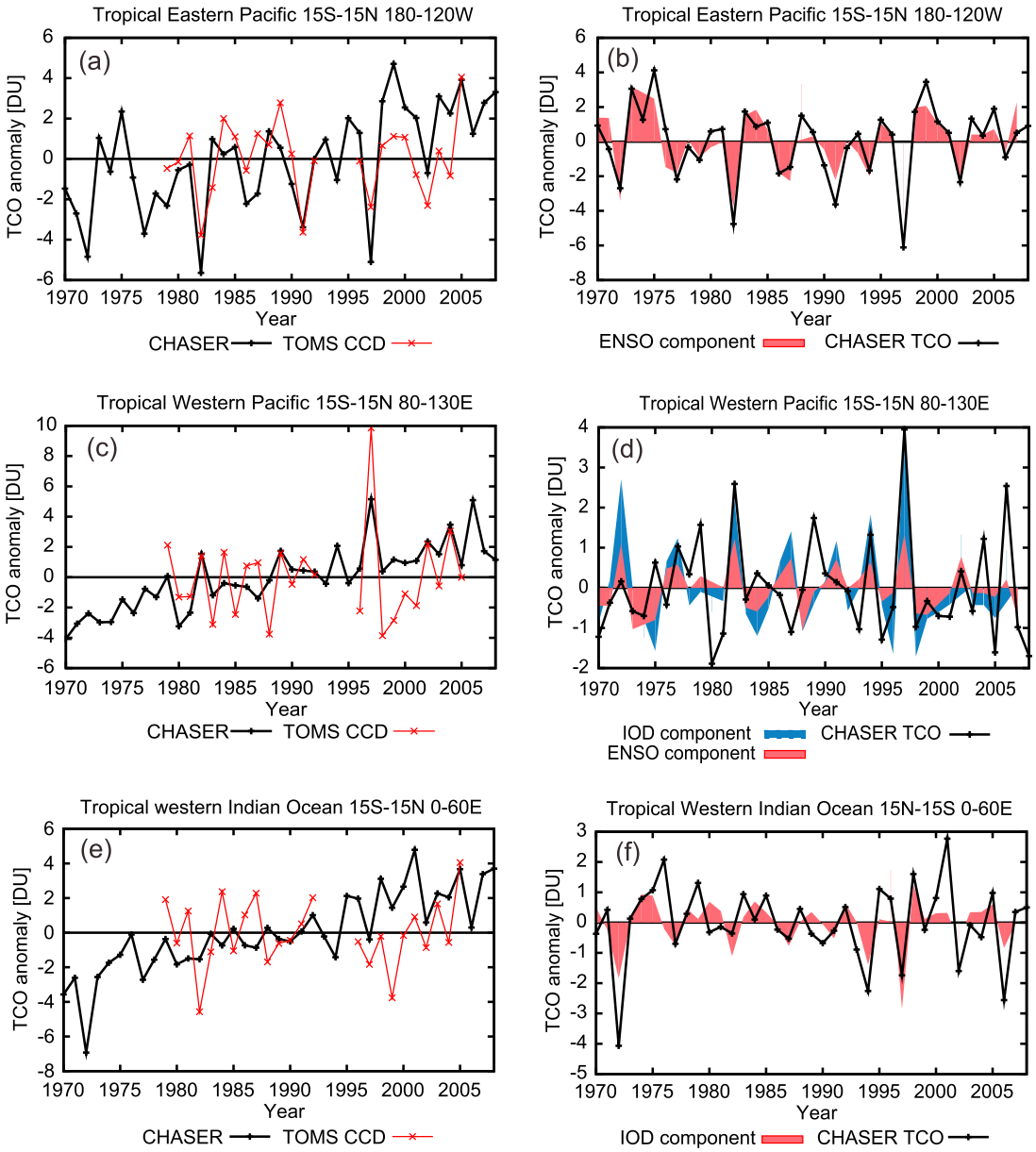

Figure 14. Time series of TCO (DU) in (a, b) the tropical eastern Pacific, (c, d) the tropical western Pacific, and (e, f) the tropical western Indian Ocean averaged for October–December. Figures 14a, 14c, and 14e show the simulated (black) and the observed (red) TCO. Observation data are derived using the TOMS convective cloud differential method in the tropics. Figures 14b, 14d, and 14f show the simulated TCO (black line) and the contribution of climate variability (red and blue) calculated from the regression coefficient and the corresponding index. The time series are calculated from the whole simulation period and are detrended to emphasize year-to-year variation rather than long-term change.

[43] Figure 15a shows interannual variation of TCO in the northwestern Indian Ocean in DJF. The simulated variation reproduces satellite-observed variation well during 1998–2008. The model, however, overestimates the observed trend. Figure 15b presents the simulated TCO anomalies, and the anomalies calculated from monsoon index (monsoon component). During 1999–2008, the simulated variation is influenced strongly by interannual variation in monsoon circulation (Figure 15b). The average contribution of the monsoon component is approximately 50%. However, the monsoon component has less impact on variation of TCO in the late 1980s and early 1990s. In addition, IOD has a non-negligible impact on TCO in the northwestern Indian Ocean in DJF.

[44] We compare the simulated TCO variation with the observation by ozonesonde (Boulder, Huntsville, and Wallops Island) in southern North America (Figure 15c) because no long-term satellite observation is sufficient to evaluate the simulated interannual variations in ozone over North America. The variation shown in Figure 15c is averaged only at the observation sites and for the days when ozonesonde was launched. The model reproduces increasing trend

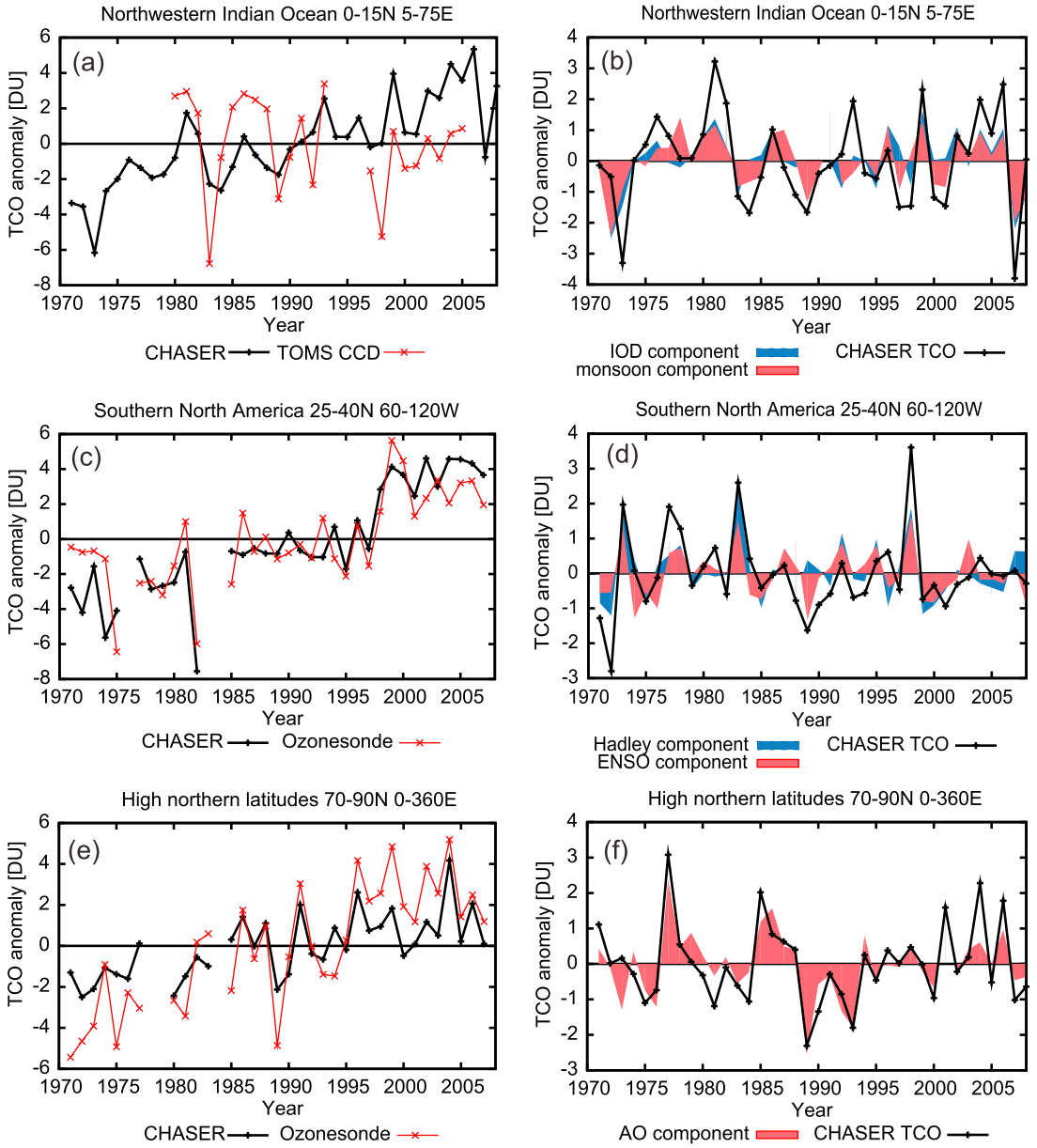

Figure 15. Same as Figure 14, but for TCO in (a, b) the northwestern Indian Ocean, (c, d) the southern North America, and (e, f) the high northern latitudes. Observation data are derived from ozonesonde (Figures 15c and 15e) in the middle to high northern latitudes. The simulated TCO shown in Figures 14c and 14e are sampled at closest time to the observation.

in TCO well. Interannual variation of TCO is generally captured by the model, in particular, between the early 1980s and the late 1990s. In this region, the ENSO component has significant impacts on TCO variation during El Niño events (Figure 15d). The contributions of ENSO were 70% in 1973, 58% in 1983, and 46% in 1998. Additionally, the Hadley component has a non-negligible impact in the region.

[45] Figure 15e shows interannual variation of the simulated TCO with ozonesonde observations (Alert, Eureka, Ny-Aalesund, Thule, and Resolute) in the high northern latitudes in DJF, as in Figure 15c. The simulated TCO variation captures the observation well after 1985. A positive trend is also reproduced by the model. Figure 15f shows that the AO component explains 72% of the variance (r = 0.85). In strong positive and negative phase years of AO (1989 and 1977), its respective contributions are 110% and 77% of the total anomaly.

5. Summary and Conclusion

[46] This study characterizes the interannual variation of global tropospheric ozone associated with meteorological variability during 1970–2008. The CHASER model generally reproduces the main features of the observed distribution and interannual variation observed by TES in late 2000s. Parts of simulated and observed interannual variation are explainable by ENSO, IOD, and AO.

[47] We investigated changes in TCO spatial patterns associated with ENSO, IOD, AO, and interannual variation in Hadley and monsoon circulations using linear regression analysis. The change associated with ENSO shows a dipole structure, which is positive anomaly (1–1.5 DU) in the western Pacific including Indonesia and negative anomaly (−2.5 DU) in the eastern Pacific in OND. This pattern is consistent with those found in previous studies [*Peters et al.*, 2001; *Doherty et al.*, 2006; *Oman et al.*, 2011]. The model also exhibits a TCO increase (0.5–1.5 DU) in the central to eastern Pacific over the subtropics during the positive phase of ENSO. The increase extends to southern North America with a 2-month lag (from 0.2 in OND to 1 DU in DJF). Additionally, we investigated the meteorological impact of ENSO more quantitatively. *Sudo and Takahashi* [2001] reported that key factors controlling ozone changes caused by meteorological change are large-scale atmospheric circulation, convection, and water vapor changes in the tropics. We further quantified the impact of atmospheric circulation and convection changes (transport), and the impact of water vapor changes (chemistry). Results show that transport has a dominant impact on the most of globe, while those of transport and chemistry are comparable in the tropical central Pacific.

[48] The pattern of TCO change induced by IOD shows a dipole structure, which is increased (1.5–2 DU) in the west of 90°E with a decrease (−1–1.5 DU) in the east during the positive phase of IOD. The mechanism causing the changes is analogous to ENSO because meteorological changes associated with IOD resemble those of ENSO. Intensified Hadley circulation causes TCO increase (up to 0.8 DU) in the Himalayas, the northeastern Pacific, and North America in DJF. The increase is probably linked to enhanced downward transport from stratosphere and upper troposphere to the lower-middle troposphere. Stronger monsoon circulation enhances TCO (1.2 DU) in the western Indian Ocean because of anomalous eastward transport of ozone from Africa. In the years of AO positive phase, TCO is decreased (−1 DU) in the high northern latitudes, reflecting weakened poleward transport from midlatitudes.

[49] Finally, we quantified the contribution of meteorological variability to total interannual variation in global and regional TCO distributions. The result suggests that interannual variation in TCO in the tropics and the high northern latitudes are generally explainable by ENSO, IOD, AO, and interannual variation in monsoon circulation. ENSO explains 33% of global TCO variance and 79% of the variance in the tropical eastern Pacific in OND. In years of strong El Niño events (1982, 1997), ENSO contributed more than 68% to negative anomalies. In the tropical western Pacific and Indonesia, both ENSO and IOD play important roles in OND. Their combinations contributed more than 84% to positive anomalies in the strong El Niño years. The relative importance of ENSO (IOD) is 56% (44%) in 1982, and is 35% (65%) in 1997. ENSO also contributes to 46–70% of the increase in southern North America for DJF in 1973, 1983, and 1998. Hadley circulation has a non-negligible impact in DJF there. In the tropical western Indian Ocean and Africa, IOD explains 36% of the variance in OND. The interannual variation of TCO in the northern Indian Ocean is influenced strongly by monsoon circulation in DJF after late 1990s. Its average contribution is about 50%. AO dominates the interannual variation of TCO in the high northern latitudes in DJF. It explains 72% of the variance, and contributes 110% (77%) of anomalies in the strongest positive (negative) phase year of AO.

[50] In this study, our simulation does not incorporate year-to-year variation in natural sources of ozone precursors (e.g., emission from wildfire, soil, vegetation) to evaluate meteorological impact on ozone apart from these emissions. However, these emissions can also be important factors controlling interannual variation in ozone. In future work, we must investigate the interannual variability of global tropospheric ozone more comprehensively, including changes in these emissions. In addition, ENSO and AO might provide a preview of future warming climate in the tropics and the northern mid-high latitude [*Yamaguchi and Noda*, 2006]. Further investigation of variation in ozone associated with them is necessary for testing changes in ozone under global warming.

[51] **Acknowledgments.** This research was supported by the Global Environment Research Fund (S-7) by the Ministry of the Environment (MOE), Japan, and the Research Program on Climate Change Adaptation (RECCA) by the Ministry of Education, Culture, Sports, Science and Technology (MEXT), Japan. We obtained NCEP/NCAR reanalysis from Web site at http://www.esrl.noaa.gov/psd/. The data sets were provided by the NOAA/OAR/ESRL PSD, Boulder, Colorado, USA. TES data were obtained from Earth Observing System Data and Information System (EOSDIS). We thank the NOAA Earth System Research Laboratory, University of Alabama at Huntsville, NASA, Wallops Island Flight Facility, Meteorological Service of Canada, Alfred Wegener Institute, Ny Alesund, and Danish Meteorological Institute for providing ozonesonde data through the WOUDC. The simulations were performed using the NIES supercomputer system.

References

Beer, R., T. A. Glavich, and D. M. Rider (2001), Tropospheric Emissions Spectrometer for the Earth Observing System Aura satellite, *Appl. Opt.*, *40*, 2356–2367, doi:10.1364/AO.40.002356.

Bowman, K. W., et al. (2006), Tropospheric Emission Spectrometer: Retrieval method and error analysis, *IEEE Trans. Geosci. Remote Sens.*, *44*(5), 1297–1307, doi:10.1109/TGRS.2006.871234.

Brasseur, G. P., M. Schultz, C. Granier, M. Saunois, T. Diehl, M. Botzet, and E. Roeckner (2006), Impact of climate change on the future chemical composition of the global troposphere, *J. Clim.*, *19*, 3932–3951, doi:10.1175/JCLI3832.1.

Chandra, S., J. R. Ziemke, W. Min, and W. G. Read (1998), Effects of 1997–1998 El Niño on tropospheric ozone and water vapor, *Geophys. Res. Lett.*, *25*(20), 3867–3870, doi:10.1029/98GL02695.

Chandra, S., J. R. Ziemke, P. K. Bhartia, and R. V. Martin (2002), Tropical tropospheric ozone: Implications for dynamics and biomass burning, *J. Geophys. Res.*, *107*(D14), 4188, doi:10.1029/2001JD000447.

Chandra, S., J. R. Ziemke, B. N. Duncan, T. L. Diehl, N. J. Livesey, and L. Froidevaux (2009), Effects of the 2006 El Niño on tropospheric ozone and carbon monoxide: Implications for dynamics and biomass burning, *Atmos. Chem. Phys.*, *9*, 4239–4249, doi:10.5194/acp-9-4239-2009.

Creilson, J. K., J. Fishman, and A. E. Wozniak (2005), Arctic Oscillation–induced variability in satellite-derived tropospheric ozone, *Geophys. Res. Lett.*, *32*, L14822, doi:10.1029/2005GL023016.

Doherty, R. M., D. S. Stevenson, C. E. Johnson, W. J. Collins, and M. G. Sanderson (2006), Tropospheric ozone and El Niño–Southern Oscillation: Influence of atmospheric dynamics, biomass burning emissions, and future climate change, *J. Geophys. Res.*, *111*, D19304, doi:10.1029/2005JD006849.

Hamid, E. Y., Z. Kawasaki, and R. Mardiana (2001), Impact of the 1997–98 El Niño event on lightning activity over Indonesia, *Geophys. Res. Lett.*, *28*(1), 147–150, doi:10.1029/2000GL011374.

Hess, P. G., and J.-F. Lamarque (2007), Ozone source attribution and its modulation by the Arctic oscillation during the spring months, *J. Geophys. Res.*, *112*, D11303, doi:10.1029/2006JD007557.

Hess, P., and N. Mahowald (2009), Interannual variability in hindcasts of atmospheric chemistry: The role of meteorology, *Atmos. Phys. Chem.*, *9*, 5261–5280, doi:10.5194/acp-9-5261-2009.

Hsu, J., M. J. Prather, and O. Wild (2005), Diagnosing the stratosphere-to-troposphere flux of ozone in a chemistry transport model, *J. Geophys. Res.*, *110*, D19305, doi:10.1029/2005JD006045.

Intergovernmental Panel on Climate Change (2007), *Climate Change 2007: The Physical Science Basis. Contribution of Working Group I to the Fourth Assessment Report of the Intergovernmental Panel on Climate Change*, edited by S. Solomon et al., Cambridge Univ. Press, Cambridge, U. K.

Kalnay, E., et al. (1996), The NCEP/NCAR 40-year reanalysis project, *Bull. Am. Meteorol. Soc.*, *77*, 437–471, doi:10.1175/1520-0477(1996)077<0437:TNYRP>2.0.CO;2.

Koumoutsaris, S., I. Bey, S. Generoso, and V. Thouret (2008), Influence of El Niño– Southern Oscillation on the interannual variability of tropospheric ozone in the northern midlatitudes, *J. Geophys. Res.*, *113*, D19301, doi:10.1029/2007JD009753.

Kulawik, S. S., J. Worden, A. Eldering, K. Bowman, M. Gunson, G. B. Osterman, L. Zhang, S. A. Clough, M. W. Shephard, and R. Beer (2006), Implementation of cloud retrievals for Tropospheric Emission Spectrometer (TES) atmospheric retrievals: 1. Description and characterization of errors on trace gas retrievals, *J. Geophys. Res.*, *111*, D24204, doi:10.1029/2005JD006733.

Kurokawa, J., T. Ohara, I. Uno, M. Hayasaki, and H. Tanimoto (2009), Influence of meteorological variability on interannual variations of springtime boundary layer ozone over Japan during 1981–2005, *Atmos. Chem. Phys.*, *9*, 6287–6304, doi:10.5194/acp-9-6287-2009.

Lamarque, J.-F., and P. G. Hess (2004), Arctic Oscillation modulation of the Northern Hemisphere spring tropospheric ozone, *Geophys. Res. Lett.*, *31*, L06127, doi:10.1029/2003GL019116.

Liu, J. J., D. B. A. Jones, S. Zhang, and J. Kar (2011), Influence of interannual variations in transport on summertime abundances of ozone over the Middle East, *J. Geophys. Res.*, *116*, D20310, doi:10.1029/2011JD016188.

Nassar, R., J. A. Logan, I. A. Megretskaia, L. T. Murray, L. Zhang, and D. B. A. Jones (2009), Analysis of tropical tropospheric ozone, carbon monoxide, and water vapor during the 2006 El Niño using TES observations and the GEOS-Chem model, *J. Geophys. Res.*, *114*, D17304, doi:10.1029/2009JD011760.

Olivier, J. G. J., J. A. van Aardenne, F. Detener, L. Ganzeveld, and J. A. H. W. Peters (2005), Recent trend in global greenhouse gas emission: Regional trends and spatial distribution of key sources, in *Non-CO_2 Greenhouse Gases (NCGG-4)*, edited by A. van Amstel, pp. 325–330, Millpress, Rotterdam, Netherlands.

Oman, L. D., J. R. Ziemke, A. R. Douglass, D. W. Waugh, C. Lang, J. M. Rodriguez, and J. E. Nielsen (2011), The response of tropical tropospheric ozone to ENSO, *Geophys. Res. Lett.*, *38*, L13706, doi:10.1029/2011GL047865.

Peters, W., M. Krol, F. Dentener, and J. Lelieveld (2001), Identification of an El Niño– Southern Oscillation signal in a multiyear global simulation of tropospheric ozone, *J. Geophys. Res.*, *106*(D10), 10,389–10,402, doi:10.1029/2000JD900658.

Pozzoli, L., G. Janssens-Maenhout, T. Diehl, I. Bey, M. G. Schultz, J. Feichter, E. Vignati, and F. Dentener (2011), Re-analysis of tropospheric sulfate aerosol and ozone for the period 1980–2005 using the aerosol-chemistry-climate model ECHAM5-HAMMOZ, *Atmos. Chem. Phys.*, *11*, 9563–9594, doi:10.5194/acp-11-9563-2011.

Price, C., and D. Rind (1992), A simple lightning parameterization for calculating global lightning distributions, *J. Geophys. Res.*, *97*(D9), 9919–9933, doi:10.1029/92JD00719.

Randel, W. J., and A. M. Thompson (2011), Interannual variability and trends in tropical ozone derived from SAGE II satellite data and SHADOZ ozonesondes, *J. Geophys. Res.*, *116*, D07303, doi:10.1029/2010JD015195.

Rayner, N. A., D. E. Parker, E. B. Horton, C. K. Folland, L. V. Alexander, D. P. Rowell, E. C. Kent, and A. Kaplan (2003), Global analyses of sea surface temperature, sea ice, and night marine air temperature since the late nineteenth century, *J. Geophys. Res.*, *108*(D14), 4407, doi:10.1029/2002JD002670.

Rodgers, C. D. (2000), *Inverse Methods for Atmospheric Sounding: Theory and Practice*, World Sci., London, doi:10.1142/9789812813718.

Saji, N. H., B. N. Goswami, P. N. Vinayachandran, and T. Yamagata (1999), A dipole mode in the tropical Indian Ocean, *Nature*, *401*, 360–363, doi:10.1038/43854.

Shapiro, M. A., H. Wernili, N. A. Bond, and R. Langland (2001), The influence of the 1997–99 El Niño Southern Oscillation on extratropical baroclinic life cycles over the eastern North Pacific, *Q. J. R. Meteorol. Soc.*, *127*, 331–342.

Spiegel, M. R. (1988), *Schaum's Outline of Theory and Problems of Statistics*, 2nd ed., 504 pp., McGraw-Hill, New York.

Sudo, K., and H. Akimoto (2007), Global source attribution of tropospheric ozone: Long-range transport from various source region, *J. Geophys. Res.*, *112*, D12302, doi:10.1029/2006JD007992.

Sudo, K., and M. Takahashi (2001), Simulation of tropospheric ozone changes during 1997–1998 El Niño: Meteorological impact on tropospheric photochemistry, *Geophys. Res. Lett.*, *28*, 4091–4094, doi:10.1029/2001GL013335.

Sudo, K., M. Takahashi, J. Kurokawa, and H. Akimoto (2002), CHASER: A global chemical model of the troposphere: 1. Model description, *J. Geophys. Res.*, *107*(D17), 4339, doi:10.1029/2001JD001113.

Sudo, K., M. Takahashi, and H. Akimoto (2003), Future changes in stratosphere- troposphere exchange and their impacts on future tropospheric ozone simulations, *Geophys. Res. Lett.*, *30*(24), 2256, doi:10.1029/2003GL018526.

Takigawa, M., M. Takahashi, and H. Akiyoshi (1999), Simulation of ozone and other chemical species using a Center for Climate System Research/National Institute for Environmental Studies atmospheric GCM with coupled stratospheric chemistry, *J. Geophys. Res.*, *104*(D11), 14,003–14,018, doi:10.1029/1998JD100105.

Tanaka, H. L., N. Ishizaki, and A. Kitoh (2004), Trend and interannual variability of Walker, monsoon and Hadley circulations defined by velocity potential in the upper troposphere, *Tellus, Ser. A*, *56*, 250–269.

van Aardenne, J. A., F. J. Dentener, J. G. J. Olivier, C. G. M. Klein Goldewijk, and J. Lelieveld (2001), A $1° \times 1°$ resolution dataset of historical anthropogenic trace gas emission for the period 1890–1990, *Global Biogeochem. Cycles*, *15*(4), 909–928, doi:10.1029/2000GB001265.

van der Werf, G. R., J. T. Randerson, L. Giglio, G. J. Collatz, P. S. Kasibhatla, and A. F. Arellano Jr. (2006), Interannual variability in global biomass burning emission from 1997 to 2004, *Atmos. Chem. Phys.*, *6*, 3423–3441, doi:10.5194/acp-6-3423-2006.

Van Leer, B. (1977), Toward the ultimate conservative difference scheme. Part IV: A new approach to numerical convection, *J. Comput. Phys.*, *23*, 276–299, doi:10.1016/0021-9991(77)90095-X.

Wang, C. (2002), Atmospheric circulation cells Associated with the El Niño–Southern Oscillation, *J. Clim.*, *15*, 399–419, doi:10.1175/1520-0442(2002)015<0399:ACCAWT>2.0.CO;2.

Wesely, M. L. (1989), Parameterization of surface resistance to gaseous dry deposition in regional-scale numerical models, *Atmos. Environ.*, *23*, 1293–1304, doi:10.1016/0004-6981(89)90153-4.

Wilks, D. S. (2006), *Statistical Methods in the Atmospheric Sciences*, 2nd ed., pp. 463–508, Academic, San Diego, Calif.

Yamaguchi, K., and A. Noda (2006), Global warming patterns over the North Pacific: ENSO versus AO, *J. Meteorol. Soc. Jpn.*, *84*(1), 221–241, doi:10.2151/jmsj.84.221.

Zeng, G., J. A. Pyle, and P. J. Young (2008), Impact of climate change on tropospheric ozone and its global budgets, *Atmos. Chem. Phys.*, *8*, 369–387, doi:10.5194/acp-8-369-2008.

Zhang, L., D. J. Jacob, X. Liu, J. A. Logan, K. Chance, A. Eldering, and B. R. Bojkov (2010), Intercomparison methods for satellite measurements of atmospheric composition: Application to tropospheric ozone from TES and OMI, *Atmos. Chem. Phys.*, *10*, 4725–4739, doi:10.5194/acp-10-4725-2010.

Zhang, L., Q. B. Li, J. Jin, H. Liu, N. Livesey, J. H. Jiang, Y. Mao, D. Chen, M. Luo, and Y. Chen (2011), Impacts of 2006 Indonesian fires and dynamics on tropical upper tropospheric carbon monoxide and ozone, *Atmos. Chem. Phys.*, *11*, 10,929–10,946, doi:10.5194/acp-11-10929-2011.

Ziemke, J. R., and S. Chandra (1999), Seasonal and interannual variabilities in tropical tropospheric ozone, *J. Geophys. Res.*, *104*(D17), 21,425–21,442, doi:10.1029/1999JD900277.

Ziemke, J. R., S. Chandra, and P. K. Bhartia (1998), Two new methods for deriving tropospheric column ozone from TOMS measurements: Assimilated UARS MLS/HALOE and convective-cloud differential techniques, *J. Geophys. Res.*, *103*(D17), 22,115–22,127, doi:10.1029/98JD01567.

Ziemke, J. R., S. Chandra, L. D. Oman, and P. K. Bhartia (2010), A new ENSO index derived from satellite measurements of column ozone, *Atmos. Chem. Phys.*, *10*, 3711–3721, doi:10.5194/acp-10-3711-2010.